JACS
JOURNAL OF THE AMERICAN CHEMICAL SOCIETY
Article
pubs.acs.org/JACS

Giant Single-Molecule Anisotropic Magnetoresistance at Room Temperature

Ji-Jun Li,[†] Mei-Lin Bai,[‡] Zhao-Bin Chen,[†] Xiao-Shun Zhou,[§] Zhan Shi,[∥] Meng Zhang,[†] Song-Yuan Ding,*[,⊥] Shi-Min Hou,*[,‡] Walther Schwarzacher,*[,#] Richard J. Nichols,[▽] and Bing-Wei Mao*[,†]

[†]State Key Laboratory of Physical Chemistry of Solid Surfaces and Department of Chemistry, College of Chemistry and Chemical Engineering, [∥]College of Materials, and [⊥]Collaborative Innovation Center of Chemistry for Energy Materials (iChEM), Xiamen University, Xiamen 361005, China

[‡]Key Laboratory for the Physics and Chemistry of Nanodevices, Department of Electronics, Peking University, Beijing 100871, China

[§]Zhejiang Key Laboratory for Reactive Chemistry on Solid Surfaces, Institute of Physical Chemistry, Zhejiang Normal University, Jinhua 321004, China

[#]HH Wills Physics Laboratory, University of Bristol, Bristol, BS8 1TL, United Kingdom

[▽]The Chemistry Department, University of Liverpool, LiverpoolL69 7ZD, United Kingdom

Supporting Information

ABSTRACT: We report an electrochemically assisted jump-to-contact scanning tunneling microscopy (STM) break junction approach to create reproducible and well-defined single-molecule spintronic junctions. The STM break junction is equipped with an external magnetic field either parallel or perpendicular to the electron transport direction. The conductance of Fe-terephthalic acid (TPA)-Fe single-molecule junctions is measured and a giant single-molecule tunneling anisotropic magnetoresistance (T-AMR) up to 53% is observed at room temperature. Theoretical calculations based on first-principles quantum simulations show that the observed AMR of Fe-TPA-Fe junctions originates from electronic coupling at the TPA−Fe interfaces modified by the magnetic orientation of the Fe electrodes with respect to the direction of current flow. The present study highlights new opportunities for obtaining detailed understanding of mechanisms of charge and spin transport in molecular junctions and the role of interfaces in determining the MR of single-molecule junctions.

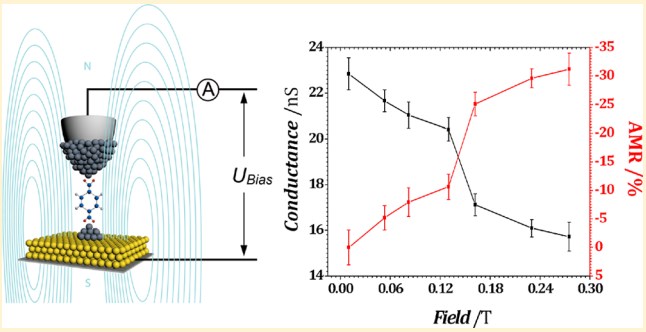

INTRODUCTION

Molecular junctions,[1−3] composed of a thin film of organic molecules contacting magnetic electrodes or single molecules bridging two magnetic electrodes, have received much attention since they have longer spin relaxation time and desirable properties, such as low cost and flexible chemical tuning of electronic functionality. This has formed two sub-branches of spintronics, namely organic spintronics[1] and single-molecule spintronics,[2,3] respectively. Single-molecule junctions provide model systems for fundamental investigation of spintronic transport, and they represent the potentially ultimate form of miniaturized spintronic devices.

For single-molecule spintronic junctions in a FM-non-magnetic molecule-FM motif, where FM refers to ferromagnetic electrode, the molecule can be considered to be a tunnel barrier in the tunneling limit. Clearly, for such junctions quantum mechanical effects will play an important role, with the spin-polarized current being crucially dependent on the magnetic state of the electrodes as well as electronic coupling between the molecule and electrodes. It was predicted in the early 2000s that simple nonmagnetic organic molecules with either conjugated or nonconjugated structures, such as 1,4-benzenedithiol (BDT)[4,5] and 1,8-octanedithiol (ODT),[6] bridging two ferromagnetic electrodes, such as Ni and Fe, should display a readily observable spin-valve type of magnetoresistance (MR), in which the electric conductance of the junctions differs when the magnetizations of the two FM layers change between the parallel and antiparallel configurations from each other. It was shown further[7] that molecules with good electron delocalization and coupling with electrodes would produce highly spin-dependent molecular conductance. These seminal theoretical works have stimulated a number of further theoretical investigations.[8−12]

However, despite much theoretical activity, reports of successful experimental work on the magnetoresistance of molecular junctions are rather limited,[13−16] and to the best of our knowledge only two or three pieces of works concerning

Received: December 9, 2014
Published: April 20, 2015

DOI: 10.1021/ja512483y
J. Am. Chem. Soc. 2015, 137, 5923−5929

single-molecule junctions[14−16] have appeared recently. In 2011 Schmaus et al.[14] reported low-temperature differential MR of cobalt (nanoisland)-(H_2Pc)-cobalt-coated tungsten tip single-molecule junctions, where H_2Pc is the nonmagnetic hydrogen phthalocyanine molecule, using spin-polarized STM operating in UHV and based on the measurement of difference in differential conductance (dI/dV) between two Co islands having parallel and antiparallel magnetization alignment, respectively, with respect to the magnetization orientation of the STM tip. In the same year, Yamada et al.[15] studied electron transport of Ni-BDT-Ni single-molecule junctions as a function of the strength and direction of the external magnetic field by using a mechanically controlled break junction (MCBJ)[17,18] at room temperature and in ambient condition. Magneto-resistance of the single-molecule junctions as large as 30% was observed. Since this was caused by the change of magnetic orientation of the external field with respect to the direction of current flow, we can term it as anisotropic magnetoresistance (AMR). However, the spin polarization of a single-molecular junction was not demonstrated in their work.

The dearth of ambient condition single-molecule MR experimental investigations, especially in comparison to the significant body of published research on large-area organic thin films,[19] is largely due to the difficulties in constructing magnetic heterojunctions with good reproducibility. Although well-established techniques in the field of molecular electronics,[17,18,20,21] such as MCBJ[17,18] and the scanning probe microscope break junction (SPM-BJ),[20,21] can enable the formation of molecular magnetic heterojunctions, they are susceptible to magnetostriction effects.[22] Also the "crash-to-contact" working principle of both the MCBJ and conventional SPM-BJ in which the electrodes are metallically fused before junction opening, precludes the formation of molecular junctions with a well-defined and reproducible structure, meaning that both the electronic structure of the junction and the magnetic state of the electrodes will show great variability even within a single set of measurements. In addition, ferromagnetic metal electrodes are prone to oxidation, which imposes difficulties for carrying out investigations under ambient conditions. These issues are unfavorable for fabricating reproducible spintronic single-molecule junctions and thus hinder the experimental investigations of important issues, such as how decisively the electronic structure of metal electrodes, localization or delocalization of bridging molecules and electronic coupling at the interfaces between them influence the MR of single-molecule junctions.

Here, we show that reproducible single-molecule spintronic junctions can be achieved by using an electrochemically assisted jump-to-contact STM-BJ approach (JTC-STM-BJ),[23,24] coupled with external magnetic fields which are either parallel or perpendicular to the direction of current flow enabling determination of the magnetic anisotropy, Figure 1. Terephthalic acid (TPA) single-molecule junctions formed with Fe electrodes are investigated, and hitherto unreported giant room temperature single-molecule AMR of up to 53% is observed. Theoretical calculations based on first-principles quantum simulations support a tunneling mechanism of AMR (T-AMR) and elucidate the importance of the electronic coupling at the TPA−Fe interfaces tuned by the direction of magnetization.

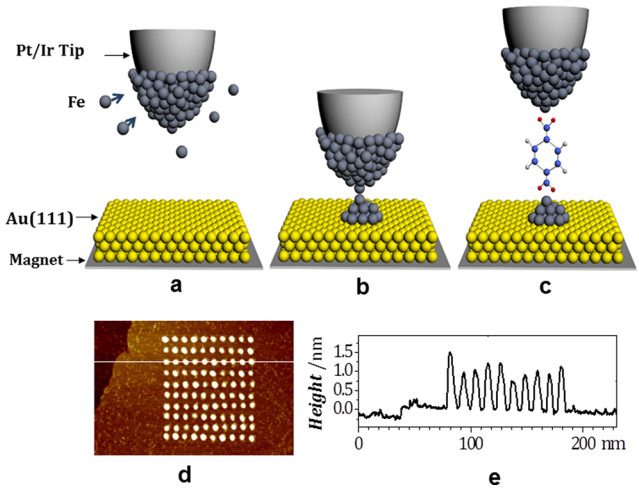

Figure 1. (a−c) Schematic illustration of operation principle of electrochemically assisted STM-BJ for spintronic investigations. Either parallel or perpendicular external magnetic field can be applied. (a) Freshly coated STM tip with a thin layer of Fe, (b) tip approaching toward the substrate surface until jump-to-contact occurs to form a nanoconstriction, and (c) stretching of the nanoconstriction and formation of molecular junctions. (d) STM image showing a (10 × 10) array (180 × 150 nm^2) Fe clusters on Au(111) created and imaged after an STM-BJ experiment. (e) Profile analysis of Fe clusters in (d).

EXPERIMENTAL SECTION

Experiments were performed on a modified Nanoscope E STM (Veeco, Santa Barbara, CA) equipped with an additional computer workstation with a DA/AD card of 16 bits, installed to control the tip movement and for data collection. For magnetoresistance measurement, the static magnetic field is applied using permanent magnets (Figures S1 and S2). Discrete magnetic field strengths can be achieved in the range from 0.010 to 0.275 T in the direction parallel to current flow. Only one magnetic field strength of 0.300 T was applied in the direction perpendicular to current flow. The Pt-Ir STM tip was mechanically cut and insulated by apiezon wax or thermosetting glue to reduce the electrochemical current. One of the {111} facets of Au single-crystal bead was used as the substrate surface. Electrochemical control was achieved through a bipotentiostat, and the electrode potentials of the STM tip and Au substrate were controlled independently. Platinum wire was used as the counter electrode and Ag/AgCl as reference electrode. Experiments were conducted in 1-butyl-3-methyl-imidazolium hexafluoroborate ($BMIPF_6$) ionic liquid[25] containing 1 mol L^{-1} $FeCl_3$ and 20 mmol L^{-1} TPA.

The procedure for creating molecular junctions with Fe includes several steps:[24] (1) Fe is continuously deposited onto the STM tip to form a thin film at 50−200 mV negative of the Nernst potential for Fe deposition, Figure 1a. (2) A preset voltage pulse is superimposed onto the voltage that is supplied by the STM instrument to the z-piezo tube. This brings the tip toward the Au(111) surface and eventually induces the jump-to-contact process. Stronger chemical interaction between Fe and Au results in the transfer of Fe atoms from the tip to the Au surface, forming a nanoconstriction of Fe between the tip and surface, Figure 1b. (3) Once the rapid rising current generated due to jump-to-contact process is detected, the tip is retracted at a typical rate of 20 nm s^{-1} until the nanoconstriction is broken. (4) The break of contact process leaves a Fe cluster on the surface and meanwhile allows nearby molecules to bridge the cluster and tip forming Fe-molecule-Fe molecular junctions. In steps 3 and 4, the conductance of the nanoconstriction and molecular junction is continuously monitored and recorded upon tip retraction at a sampling frequency of 20 kHz to generate a conductance trace as a function of retraction distance. The above procedure was repeated thousands of times per experiment, each time at a new location. Each experiment was repeated several

DOI: 10.1021/ja512483y
J. Am. Chem. Soc. 2015, 137, 5923−5929

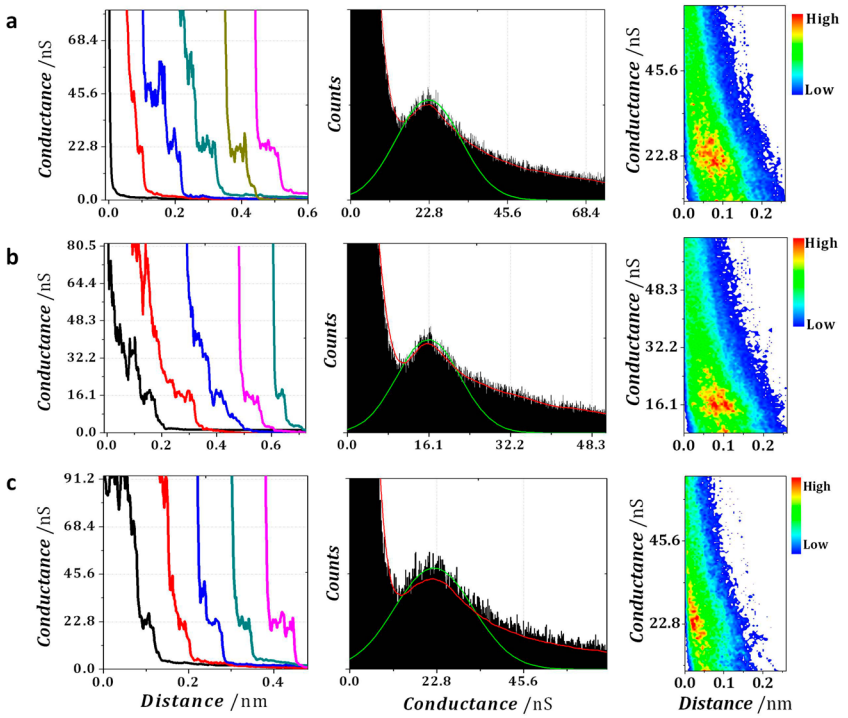

Figure 2. Typical conductance traces (left panels) and histograms (middle panels) of Fe-TPA-Fe molecular junctions in the absence (a) and presence of parallel (b, 0.230 T) and perpendicular (c, 0.300 T) magnetic field. The right panels are the two-dimensional histograms of conductance and displacement distance. Solution: $BMIPF_6$ containing 1 mol L^{-1} $FeCl_3$ and 20 mmol L^{-1} TPA. The potentials of the substrate Au(111) and the tip are −750 and −850 mV vs Ag/AgCl, respectively, which generate a bias of −100 mV (tip positive). The selection rate of conductance traces for construction of histograms is 17% (1577 out of 9297), 22% (2136 out of 9552), and 13% (713 out of 5550) for the absence of magnetic field and parallel and perpendicular magnetic fields, respectively.

times. Histograms were constructed based on the conductance traces after removing those which are very noisy or show exponential decay with no step in the desired conductance range, and the most probable conductance was determined by Gaussian fitting for each condition.

Spanish initiative for electronic simulations with thousands of atoms (SIESTA) code[26] was used to compute the atomic structure of Fe-TPA-Fe molecular junctions and the quantum transport code spin and molecular electronics algorithm on a generalized atomic orbital landscape (SMEAGOL)[7,27] to study their electronic transport properties. SIESTA is an efficient DFT package, which makes use of improved Troullier−Martins pseudopotentials for describing the atomic cores and adopts a finite-range numerical orbital basis set to expand the wave functions of the valence electrons.[26,28] A double-ζ plus polarization basis set is used for H, C, and O, while a single-ζ plus polarization basis is used for Fe and Au. The exchange−correlation functional is at the level of the generalized gradient approximation within the Perdew−Burke−Ernzerhof formulation.[29] Geometry optimization is performed by standard conjugate gradient relaxation until the atomic forces are smaller than 0.03 eV $Å^{-1}$.

SMEAGOL is a practical implementation of the NEGF + DFT approach, which employs SIESTA as the DFT platform.[7,30] An equivalent cutoff of 200 Ryd for the real space grid was used. The charge density was integrated over 36 energy points along the semicircle, 36 along the line in the complex plane, while 36 poles are used for the Fermi function (the electronic temperature was 25 meV). Periodic boundary conditions in the plane transverse to the transport were always considered. The unit cell of the extended molecule comprises TPA molecule and several layers of the electrodes. The total transmission coefficient $T(E)$ of the junction was evaluated as

$$T(E) = \frac{1}{\Omega_{2DBZ}} \int_{2DBZ} T(\vec{k}; E)d\vec{k} \quad (1)$$

where Ω_{2DBZ} is the area of the two-dimensional Brillouin zone (2DBZ) in the transverse directions. The k-dependent transmission coefficient is obtained as

$$T(\vec{k}, E) = Tr[\Gamma_L G_M^R \Gamma_R G_M^{R+}] \quad (2)$$

where G_M^R is the retarded Green's function matrix of the extended molecule and Γ_L (Γ_R) is the broadening function matrix describing the interaction of the extended molecule with the left-hand (right-hand) side electrode. Here, we calculate the transmission coefficient by sampling 3 × 5 k-points in the transverse 2DBZ.

RESULTS AND DISCUSSION

The principle of the JTC-STM-BJ approach to construct a single-molecule spintronic junction is illustrated schematically in Figure 1. Fe clusters can be repeatedly created at different locations of the surface and Figure 1d shows an array of (10 × 10) Fe clusters. The clusters have sizes of about 8−10 nm in diameter and 1−1.5 nm in height, corresponding to roughly 6000 Fe atoms per cluster. An array size of up to (100 × 100) can be easily achieved with reasonably uniform size. The importance of the jump-to-contact strategy is two-fold. First, the Fe clusters have well-defined crystalline structure which in turn establishes the surface structure of the substrate;[31,32] this observation is supported by atom dynamics simulations.[33] Second, the Fe clusters are single domain ferromagnetic particles with strong shape anisotropy. Comparison of the shape anisotropy energy with the thermal energy suggests that Fe clusters having a size of 8 × 8 × 1 nm^3 are in the anisotropic superparamagnetic regime at room temperature.[34] This means that on the one hand, the magnetic moment of the cluster can be manipulated by the external magnetic field, while on the other hand, it stays in-plane with zero average strength in the

DOI: 10.1021/ja512483y
J. Am. Chem. Soc. 2015, 137, 5923−5929

absence of a field because of the strong out-of-plane demagnetizing factor (Note S2). Micromagnetic simulations have been carried out using the NMAG code,[35] and results show that the Fe cluster can be magnetized to near saturation by an external field of low strength in the presence of a Fe tip that is placed closely above the cluster, Figure S3. This means that these Fe clusters can serve as one of the magnetic electrodes necessary to form molecular spintronic junctions.

TPA is a short molecule with a length of ca. 0.8 nm, whose electronic structure and molecule conformation resemble those of benzenedithiol (BDT). The latter is regarded as a model system and features in many theoretical investigations[4,5,36,37] with the consensus that electron transport follows a super-exchange mechanism. To serve as a reference point, Fe-TPA-Fe molecular junctions in the absence of external magnetic field are studied first. The STM tip retraction traces are shown in Figure 2a (left panel) as junction conductance versus distance curves. These feature plateaus and steps are synonymous with the formation of molecular junctions. The lowest conductance plateau located at around 22.8 nS corresponds to the conductance of the Fe-TPA-Fe single-molecule junction. Many of these curves from many retraction events are represented in conductance histograms (Figure 2a, middle panel). The Gaussian fitting of the conductance histogram, in Figure 2a middle panel, further verifies the most probable single-molecule conductance of 22.8 ± 0.7 nS. A two-dimensional histogram of conductance and stretching distance is also constructed, right panel, and the high count region of conductance and length gives the most probable junction conductance and displacement distance.

Applying a perpendicular magnetic field (of up to 0.300 T) does not cause a change in the conductance of Fe-TPA-Fe single-molecule junctions, Figure 2c. Surprisingly, however, application of a parallel magnetic field of 0.230 T decreases their conductance to 16.1 ± 0.4 nS, as seen in Figure 2b. This corresponds to an AMR of 30% at the field strength of 0.23 T and bias of 0.1 V (tip positive). Here, AMR is defined as AMR = $(G_{per} - G_{para})/G_{per}$, where G_{per} and G_{para} are, respectively, the conductance values of Fe-molecule-Fe single-molecule junctions under perpendicular and parallel magnetic field.

Several pieces of evidence are worth mentioning to support the reliability of the measured conductance data: (1) The most probable conductance values obtained from histograms constructed from at least five experiments, each containing more than 1000 conductance traces, show small standard deviations as shown by the small error bars; (2) the addition of more sets of conductance traces to a specified conductance histogram does not change the most probable value of conductance although the height of the conductance peak increases (Figure S4); and (3) experiments performed with a Cu-TPA-Cu molecular junction do not show any obvious change of conductance regardless of magnetic field direction and strength (Figure S5).

It is also important to note that in the present work discrete and static parallel magnetic fields are applied using a set of permanent magnets so that the Fe electrodes are always magnetized from remanent field strength (~0.010 T) to the specified field strength before measurements. Although this manner of magnetic field variation does not allow studies of MR hysteresis, it eliminates artifacts due to magnetostriction, because the tip and cluster magnetization and therefore the magnetostriction do not change, while the molecular conductance is measured.

We then focused on the parallel magnetic field and further studied the AMR of the molecular junction with a set of seven magnets that provide applied magnetic fields in the range of 0.010 to 0.275 T. We mention that the remnant magnetic field from the STM sample stage is 0.010 T due to a permanent magnet placed under the STM cell and used to fix the STM head. The corresponding conductance traces and two-dimensional histogram are provided in Figure 3. Increasing the

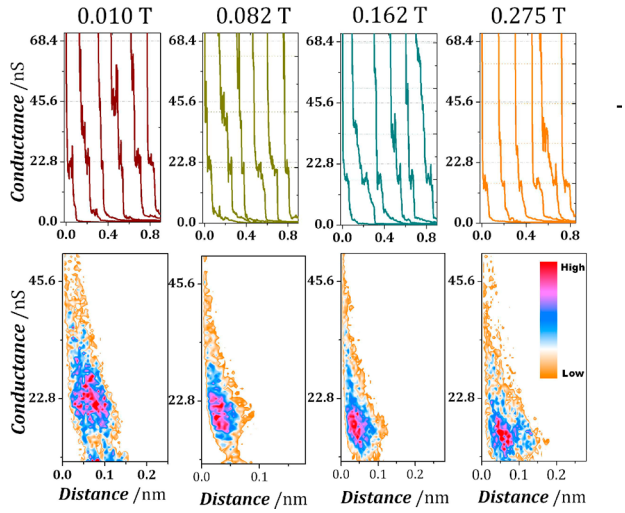

Figure 3. Conductance traces (upper panels) and two-dimensional histograms (lower panels) of Fe-TPA-Fe molecular junctions with four strength of parallel magnetic fields. The selection rate is of 17% for 0.01 T, 16.9% for 0.082 T, 18.8% for 0.162 T, and 22.5% for 0.275 T, respectively.

strength of parallel magnetic field causes gradual decrease of the single-molecule conductance. The curves presented in Figure 4a are plots of the single-molecule conductance and AMR as a

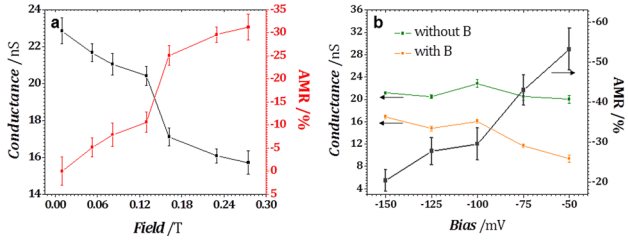

Figure 4. Single-molecule conductance and AMR as a function of parallel magnetic field strength at a bias voltage of −0.1 V (a) and a function of bias voltage under a parallel magnetic field strength of 0.230 T (b).

function of magnetic field strength at a bias voltage of 0.1 V. Each error bar is the standard deviation of five sets of most probable conductance data at the specified magnetic field strength. A clear monotonic decrease of conductance, or equivalently an increase of AMR, with increasing magnetic field strength is seen.

The applied bias voltage can influence the electric current through the junction by altering the conducting states in the bias window as well as the alignment between the metal Fermi levels and frontier molecular orbitals of the molecular bridge. We studied the bias dependence of the conductance under a parallel magnetic field strength of 0.230 T. Note that to maintain a fixed rate of Fe deposition on the tip, the bias is

DOI: 10.1021/ja512483y
J. Am. Chem. Soc. 2015, 137, 5923−5929

varied by changing the substrate potential while keeping the tip potential fixed, and only negative biases (tip vs substrate) are possible to avoid bulk deposition of Fe on the substrate. Furthermore, to separate the bias influence from the influence of electrode potential, normalization of AMR is performed by subtracting the conductance without field G_{zero} from that with parallel field G_{para} at each bias voltage, followed by dividing G_{zero} at the same bias voltage. Figure 4b shows that the normalized AMR decreases with increasing bias voltage. An AMR as high as 53 ± 5% is reached at a bias of −50 mV, which decays rapidly as the bias voltage increases in the low bias regime (−50 ∼ −100 mV) and slightly levels off in the high bias regime (−100 ∼ −150 mV). Such an AMR-bias dependency is seen regardless of magnetic field strength.

The most important observations of the present study are that the Fe-TPA-Fe single-molecule junctions exhibit a giant AMR (up to 53 ± 5%), i.e., the conductance of the molecular junctions under a parallel magnetic field is much lower than that under a perpendicular field, and the AMR increases as the magnetic field is increased or the bias voltage is decreased. However, TPA is a simple nonmagnetic organic molecule for which electron transport is expected to be by the super-exchange mechanism. By itself, it is not expected to give rise to AMR. This implies that not only is the spin polarization of the pair of magnetic electrodes but also the electronic coupling at the interface between TPA and the nanoscale Fe electrodes crucial to the observation of AMR of Fe-TPA-Fe molecular junctions.[38] For the spin polarization of the Fe electrodes, we propose that the single domain Fe clusters have an in-plane magnetic moment which averages to zero within the time scale of measurement (∼10 ms) in the absence of an external magnetic field at room temperature, Figure 5a; while the Fe

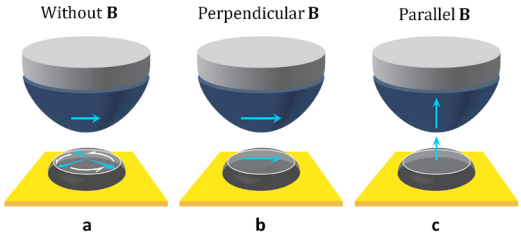

Figure 5. Schematic illustration of proposed magnetization orientation of cluster and film electrodes of Fe (a) in the absence of magnetic field and (b) with field perpendicular and (c) parallel to the direction of current flow. The blue arrows represent the magnetization. Refer to Note S2.

thin film coating the tip either has an in-plane magnetic orientation[39] in the absence of a magnetic field or follows the direction of the externally applied magnetic field. This would lead to the following scenario: Both in the absence of magnetic field and in the presence of a perpendicular external magnetic field, the cluster and film electrodes both have in-plane magnetic orientation, Figure 5a,b. Rotating the external magnetic field to the parallel direction changes the magnetization of the two electrodes into an out-of plane orientation, which is parallel to the current flow. Together with the well-defined junction structure reproducible and reliable AMR measurements of FM-molecule-FM single-molecule spintronic junctions could be ensured.

In order to gain an in-depth insight into the origin of the AMR of the Fe-TPA-Fe molecular junctions, we have theoretically investigated the effects of the magnetic orientation on the electronic transport properties of single TPA molecules connected to Fe electrodes. This is realized by employing the nonequilibrium Green's function formalism combined with density functional theory (i.e., the NEGF + DFT approach).[7,27] Crucially, spin−orbit coupling is taken into account through pseudopotentials.[30,40] We first consider a simple model system in which one TPA molecule is connected to two semi-infinite Fe monatomic chains (see Figure S7). Indeed, the transmission around the Fermi level shows a difference when the magnetic orientation is changed, although the overall shape of the transmission spectrum remains largely unchanged. In detail, the transmission spectrum around the Fermi level is very flat when the magnetization is parallel to the transport (the z-axis), and the transmission coefficient at the Fermi level is calculated to be 4.3×10^{-2}. In contrast, when the magnetization is perpendicular to the transport (the x-axis), the transmission coefficient increases from 4.9×10^{-2} at the Fermi level to 0.28 at 62 meV above the Fermi level. This tuning of the transmission coefficients around the Fermi level by rotating the magnetization direction is in qualitative agreement with our experimental results for the Fe-TPA-Fe molecular junctions.

Encouraged by this preliminary yet favorable result, we constructed more realistic junction models with bulk Fe electrodes for detailed analysis. Considering that in our experiments one of the Fe electrodes composing the Fe-TPA-Fe junction is a Fe cluster created in situ on the Au(111) surface and that Fe always exhibits a pseudomorphic growth behavior on the flat Au(111) surface when its thickness is below a critical value,[41] an asymmetric TPA junction is constructed, in which one electrode is bulk BCC Fe with the (110) orientation and the other is bulk FCC Au with two monolayers of Fe pseudomorphically grown on the (111) surface. As shown in Figure 6a (see also Figure S8), at one side of the Au/Fe-TPA-Fe junction the TPA molecule is assumed to connect to the Fe(110) surface through a two-atom Fe cluster mimicking a Fe monatomic chain, while at the other side, the TPA molecule is wired to the Au/Fe(111) electrodes through a five-atom Fe cluster. The equilibrium transmission spectra of the asymmetric Au/Fe-TPA-Fe junction are presented in Figure 6b,c. Similarly to the case of Fe monatomic chain electrodes, the magnetization direction does not affect the overall shape of the transmission spectra, but in the energy range 0.1 to 0.5 eV above the Fermi level the transmission coefficients calculated for the magnetization perpendicular to the transport are larger than those for the magnetization lying parallel to the transport. Note that during the conductance measurements, the electrode potentials of the pair of Fe electrodes are gated, by the reference/counter electrode combination, to be 50−200 mV negative of the equilibrium potential. In other words, the energies of electrons at the Fe electrode are shifted by 50−200 mV above the Fermi level at equilibrium, into the energy region that shows a significant effect of magnetic orientation on the transmission coefficient in Figure 6c. The calculated effect of magnetic orientation on the transmission coefficient is in good qualitative agreement with experimental observations. These differences in the transmission curves originate from the dependence of the local density of states (LDOS) of the Fe atoms connected directly with the TPA molecule on the magnetization orientation, Figure 6d. When comparing the LDOS of the two Fe apex atoms (labeled as Fe1 and Fe2) with the transmission spectra of the asymmetric Au/Fe-TPA-Fe junction, it is found that the LDOS of the $3d_{yz}$ orbital of the Fe apex atom on the Au/

DOI: 10.1021/ja512483y
J. Am. Chem. Soc. 2015, 137, 5923−5929

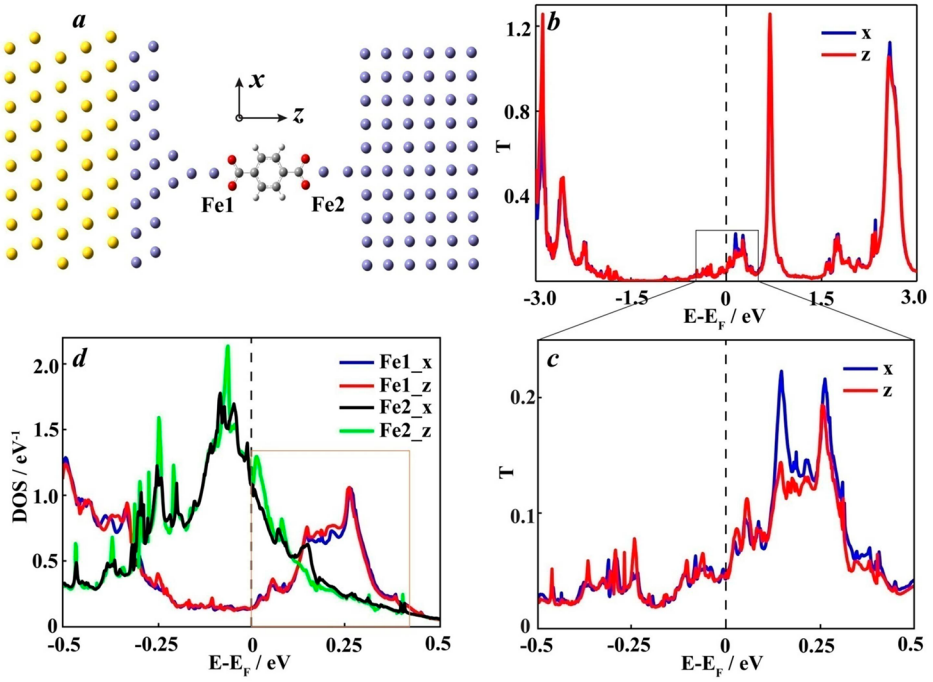

Figure 6. Atomic structure and transport properties of the asymmetric Au/Fe-TPA-Fe molecular junction. (a) The optimized geometric structure of Au/Fe-TPA-Fe junction with four atoms arranged in a tetrahedral configuration plus one outside atom connecting to the apex, (b) equilibrium transmission spectra on a large energy scale and (c) around the Fermi level and (d) the LDOS of the $3d_{yz}$ orbital of the two Fe tip atoms.

Fe(111) surface determines the shape of the transmission spectra in the energy range from 0.1 to 0.5 eV, while the LDOS of the $3d_{yz}$ orbital of the Fe apex atom on the Fe(110) surface determines the relative magnitude of the transmission in the same energy range. This illustrates the important role played by the fine structure of the TPA-Fe interfaces. In fact, a number of configurations of molecular junctions have been constructed for calculation including those with two Fe electrodes having the (100) or (110) surfaces of the bulk BCC structure (see Figures S10 and S11) for which no significant AMR is obtained. This further reveals the vital importance of the interfacial structure of the single-molecule junction for the observation of AMR.[38]

It should be noted, however, that the calculated transmission coefficients are much larger than the measured conductance. Further theoretical investigations are needed to clarify the underlying factors which cause such a discrepancy. Nevertheless, the calculations clearly show that the spin−orbit interaction is dependent on the magnetization orientation of the Fe electrode and can influence the LDOS of the contact and hence the tunneling probability through the Fe-TPA-Fe single-molecule junctions. Such an influence has not been studied theoretically for room temperature single-molecule spintronic junctions previously, but our explanation is supported by the tunneling AMR reported for large-area organic spintronic devices.[42,43] Thus, both experiment and theory reveal that the observed AMR of Fe-TPA-Fe single-molecule junctions is tunneling AMR (T-AMR).

CONCLUSIONS

We have demonstrated that reproducible Fe-TPA-Fe single-molecule spintronic junctions can be constructed by a JTC-STM-BJ approach at room temperature. This has led to the observation of hitherto unreported tunneling AMR of single-molecule junctions, which is as large as >53% at room temperature and tip bias of −50 mV. The advantages of precise control of the chemical state of the magnetic electrodes and the creation of nanoconstrictions and metal-molecule contacts with well-defined structures as well as greatly reduced magnetostriction make the JTC-STM-BJ a powerful room temperature experimental platform for constructing robust single-molecule spintronic junctions including magnetic or nonmagnetic electrodes contacting magnetic or nonmagnetic molecules. This provides the potential for seeking and investigating diverse single-molecule spintronic systems given the availability of various kinds of designable molecules. For example, using the JTC-STM-BJ a preliminary study on the effect of bromide substitution on the conductance of TPA (2,3,5,6-tetrabromoterephthalic acid, TPA-Br_4) molecular junctions has been carried out. The introduction of the four electron-withdrawing Br atoms causes extended delocalization of electrons through the benzene skeleton so that TPA-Br4 molecular junctions exhibit larger electric conductance than TPA molecular junctions under the same condition, Figure S12. The presence of the Br atoms also influences the electronic coupling at the contact. These two factors together result in an observation of AMR of 38.7%, which is bigger than that of TPA (29.4%) under the same condition (tip bias −100 mV and parallel magnetic field of 0.23 T). Systematic and comparative studies of the AMR of saturated and conjugated molecular spintronic junctions are currently in progress in our laboratories.

ASSOCIATED CONTENT

Supporting Information

Descriptions of the experimental and calculation details. The Supporting Information is available free of charge on the ACS Publications website at DOI: 10.1021/ja512483y.

AUTHOR INFORMATION

Corresponding Authors

*bwmao@xmu.edu.cn

DOI: 10.1021/ja512483y
J. Am. Chem. Soc. 2015, 137, 5923−5929

*smhou@pku.edu.cn
*W.Schwarzacher@bristol.ac.uk
*syding@xmu.edu.cn

Notes

The authors declare no competing financial interest.

■ ACKNOWLEDGMENTS

We are grateful to Profs. D. L. Peng at Xiamen University, D. Wei at Qinghua University, and J. Shen at Fudan University for helpful discussions. We also thank Mr. Lei Xu at Peking University for his effort in attempting for micromagnetic simulations. This work is supported by the National Science Foundation of China (21033007, 20121002, and 61321001) and MOST of China under the 973 (2012CB932902, 2013CB933404), and R.J.N. and W.S. acknowledge the financial support of EPSRC under the grants EP/H001980/1 and EP/H002227/1.

■ REFERENCES

(1) Naber, W. J. M.; Faez, S.; van der Wiel, W. G. *J. Phys. D: Appl. Phys.* **2007**, *40*, R205−R228.
(2) Sanvito, S. *Chem. Soc. Rev.* **2011**, *40*, 3336−3355.
(3) Sanvito, S.; Rocha, A. R. *J. Comput. Theor. Nanosci.* **2006**, *3*, 624−642.
(4) Emberly, E. G.; Kirczenow, G. *Chem. Phys.* **2002**, *281*, 311−324.
(5) Pati, R.; Senapati, L.; Ajayan, P. M.; Nayak, S. K. *Phys. Rev. B* **2003**, *68*, 100407.
(6) Dalgleish, H.; Kirczenow, G. *Phys. Rev. B* **2005**, *72*, 184407.
(7) Rocha, A. R.; Garcia-Suarez, V. M.; Bailey, S. W.; Lambert, C. J.; Ferrer, J.; Sanvito, S. *Nat. Mater.* **2005**, *4*, 335−339.
(8) Waldron, D.; Haney, P.; Larade, B.; MacDonald, A.; Guo, H. *Phys. Rev. Lett.* **2006**, *96*, 166804.
(9) He, H.; Pandey, R.; Karna, S. P. *Chem. Phys. Lett.* **2006**, *428*, 411−415.
(10) Rocha, A. R.; Sanvito, S. *J. Appl. Phys.* **2007**, *101*, 09B102.
(11) Wang, Y.; Che, J. G.; Fry, J. N.; Cheng, H.-P. *J. Phys. Chem. Lett.* **2013**, *4*, 3508−3512.
(12) Wagner, S.; Kisslinger, F.; Ballmann, S.; Schramm, F.; Chandrasekar, R.; Bodenstein, T.; Fuhr, O.; Secker, D.; Fink, K.; Ruben, M.; Weber, H. B. *Nat. Nanotechnol.* **2013**, *8*, 575−579.
(13) Petta, J. R.; Slater, S. K.; Ralph, D. C. *Phys. Rev. Lett.* **2004**, *93*, 136601.
(14) Schmaus, S.; Bagrets, A.; Nahas, Y.; Yamada, T. K.; Bork, A.; Bowen, M.; Beaurepaire, E.; Evers, F.; Wulfhekel, W. *Nat. Nanotechnol.* **2011**, *6*, 185−189.
(15) Yamada, R.; Noguchi, M.; Tada, H. *Appl. Phys. Lett.* **2011**, *98*, 053110.
(16) Horiguchi, K.; Sagisaka, T.; Kurokawa, S.; Sakai, A. *J. Appl. Phys.* **2013**, *113*, 4800530.
(17) Agrait, N.; Yeyati, A. L.; van Ruitenbeek, J. M. *Phys. Rep.* **2003**, *377*, 81−279.
(18) Mantooth, B. A.; Weiss, P. S. *Proc. IEEE* **2003**, *91*, 1785−1802.
(19) Watanabe, S.; Ando, K.; Kang, K.; Mooser, S.; Vaynzof, Y.; Kurebayashi, H.; Saitoh, E.; Sirringhaus, H. *Nat. Phys.* **2014**, *10*, 308−313.
(20) Tao, N. J. *Nat. Nanotechnol.* **2006**, *1*, 173−181.
(21) Xu, B. Q.; Tao, N. J. J. *Science* **2003**, *301*, 1221−1223.
(22) Brumfiel, G. *Nature* **2003**, *426*, 110−110.
(23) Kolb, D. M.; Ullmann, R.; Will, T. *Science* **1997**, *275*, 1097−1099.
(24) Zhou, X.-S.; Wei, Y.-M.; Liu, L.; Chen, Z.-B.; Tang, J.; Mao, B.-W. *J. Am. Chem. Soc.* **2008**, *130*, 13228−13230.
(25) Su, Y. Z.; Fu, Y. C.; Wei, Y. M.; Yan, J. W.; Mao, B. W. *ChemPhysChem* **2010**, *11*, 2764−2778.
(26) Soler, J. M.; Artacho, E.; Gale, J. D.; Garcia, A.; Junquera, J.; Ordejon, P.; Sanchez-Portal, D. *J. Phys.: Condens. Matter* **2002**, *14*, 2745−2779.
(27) Rocha, A. R.; Garcia-Suarez, V. M.; Bailey, S.; Lambert, C.; Ferrer, J.; Sanvito, S. *Phys. Rev. B* **2006**, *73*, 085414.
(28) Troullier, N.; Martins, J. L. *Phys. Rev. B* **1991**, *43*, 1993−2006.
(29) Perdew, J. P.; Burke, K.; Ernzerhof, M. *Phys. Rev. Lett.* **1996**, *77*, 3865−3868.
(30) Fernandez-Seivane, L.; Oliveira, M. A.; Sanvito, S.; Ferrer, J. *J. Phys.: Condens. Matter* **2006**, *18*, 7999−8013.
(31) Wei, Y.-M.; Liang, J.-H.; Chen, Z.-B.; Zhou, X.-S.; Mao, B.-W.; Oviedo, O. A.; Leiva, E. P. M. *Phys. Chem. Chem. Phys.* **2013**, *15*, 12459−12465.
(32) Liang, J.; Liu, L.; Gao, Y.; Wei, Y.; Chen, Z.; Zhou, X.; Zhao, J.; Mao, B. *J. Electroanal. Chem.* **2013**, *688*, 257−261.
(33) Mariscal, M.; Narambuena, C. F.; Del Popolo, M. G.; Leiva, E. P. M. *Nanotechnology* **2005**, *16*, 974−980.
(34) Bedanta, S.; Kleemann, W. *J. Phys. D: Appl. Phys.* **2009**, *42*, 013001.
(35) Fischbacher, T.; Franchin, M.; Bordignon, G.; Fangohr, H. *IEEE Trans. Magn.* **2007**, *43*, 2896−2898.
(36) Salomon, A.; Cahen, D.; Lindsay, S.; Tomfohr, J.; Engelkes, V. B.; Frisbie, C. D. *Adv. Mater.* **2003**, *15*, 1881−1890.
(37) Reed, M. A.; Zhou, C.; Muller, C. J.; Burgin, T. P.; Tour, J. M. *Science* **1997**, *278*, 252−254.
(38) Sanvito, S. *Nat. Phys.* **2010**, *6*, 562−564.
(39) Toulemonde, O.; Petrov, V.; Abdi, A. N.; Bucher, J. P. *J. Appl. Phys.* **2004**, *95*, 6565−6567.
(40) Zhang, R.; Ma, G.; Li, R.; Qian, Z.; Shen, Z.; Zhao, X.; Hou, S.; Sanvito, S. *J. Phys: Condens. Matter* **2009**, *21*, 335301.
(41) Allmers, T.; Donath, M. *New J. Phys.* **2009**, *11*, 103049.
(42) von Bergmann, K.; et al. *Phys. Rev. B* **2012**, *86*, 134422.
(43) Grunewald, M.; Wahler, M.; Schumann, F.; Michelfeit, M.; Gould, C.; Schmidt, R.; Wurthner, F.; Schmidt, G.; Molenkamp, L. W. *Phys. Rev. B* **2011**, *84*, 125208.

DOI: 10.1021/ja512483y
J. Am. Chem. Soc. 2015, 137, 5923−5929